# A Water-Soluble Redox-Active Cage Hosting Polyoxometalates for Selective Desulfurization Catalysis

Li-Xuan Cai, Shao-Chuan Li, Dan-Ni Yan, Li-Peng Zhou, Fang Guo, and Qing-Fu Sun

*J. Am. Chem. Soc.*, **Just Accepted Manuscript** • DOI: 10.1021/jacs.8b00394 • Publication Date (Web): 13 Mar 2018

# A Water-Soluble Redox-Active Cage Hosting Polyoxometalates for Selective Desulfurization Catalysis

Li-Xuan Cai,[†] Shao-Chuan Li,[†,‡] Dan-Ni Yan,[†,§] Li-Peng Zhou,[†] Fang Guo,[‡] Qing-Fu Sun*[†]

[†]State Key Laboratory of Structural Chemistry, Fujian Institute of Research on the Structure of Matter, Chinese Academy of Sciences, Fuzhou 350002, PR China

[‡]College of Chemistry, Liaoning University, Shenyang 110036, PR China

[§]University of Chinese Academy of Sciences, Beijing 100049, PR China

*KEYWORDS. Self-assembly; Cage; Redox; Water-soluble; Encapsulation; Desulfurization.*

**ABSTRACT:** Transformations within container-molecules provide a good alternative between traditional homogeneous and heterogeneous catalysis, as the containers themselves can be regarded as single molecular nanomicelles. We report here the designed-synthesis of a water-soluble redox-active supramolecular $Pd_4L_2$ cage and its application in the encapsulation of aromatic molecules and polyoxometalates (POMs) catalysts. Compared to the previous known $Pd_6L_4$ cage, our results show that replacement of two cis-blocked palladium corners with p-xylene bridges through pyridinium bonds formation between the 2,4,6-tri-4-pyridyl-1,3,5-triazine (TPT) ligands not only provides reversible redox-activities for the new $Pd_4L_2$ cage, but also realizes the expansion and subdivision of its internal cavity. An increased number of guests, including polyaromatics and POMs, can be accommodated inside the $Pd_4L_2$ cage. Moreover, both conversion and product selectivity (sulfoxide over sulfone) have also been much enhanced in the desulfurization reactions catalyzed by the POMs@$Pd_4L_2$ host-guest complexes. We expect that further photochromic and/or photoredox functioins are possible taking advantage of this new generation of organo-palladium cage.

## INTRODUCTION

Development of functional container-molecules has received increased attention in the past decades, due to the unique properties and behaviors of the guest molecules confined within the nanospace.[1] Guest encapsulations within the nanocontainer are mainly through noncovalent interactions, such as electrostatic attraction, hydrophobic effect, π-π stacking, hydrogen bonding et al.[2] Thus, rational design and modulation on the size, shape, and the electronic properties of the nano-containers are of key importance in order to realize binding/catalytic transformations of guest species inside the confined space.[2e,3]

Pyridinium functionalization has been proven as a promising and powerful approach in the construction of multi-cationic self-assembled host.[4] Pioneering works by Stoddart and coworders[5] have elucidated the vital role of pyridinium moieties in establishing the functions of macrocycles and cages because of their unique electrostatic and redox properties, like $CBPQT^{4+}$, $Ex^nBox^{4+}$, $ExCage^{6+}$, $BlueCage^{6+}$. Encapsulation of cyclobis(paraquat-p-phenylene) ($CBPQT^{4+}$) by the $Pd_{12}L_{24}$ molecular flask charged with endohedral 1,5-dioxynaphthalene (DNP) units has been demonstrated, where electrolyte stimulus can act as a gate leading to emergent binding properties.[6] Recently, Yoshizawa et al has reported a $Pd_2L_4$ molecular capsule enclosed by eight redox-active dihydrophenazine panels, which can be converted into a stable tetra-radical-cationic capsule by electrochemical or chemical oxidation.[7]

Polyoxometalates (POMs) are a unique family of discrete metal−clusters and have various applications ranging from catalysis, medicine, electrochemistry, photochromism, to magnetism.[8] However, it is still a big challenge to introduce POMs into a supramolecular host, as a result of the small cavities and the instability of the known container-molecules. POM@cage complexes have been rarely reported[5a,8a,9] and to the best of our knowledge, catalytic activity of such host-guest complexes has never been explored.

**SCHEME 1**. $Pd_4L_2$ Nanocage and its near relative $Pd_6L_4$ cage.

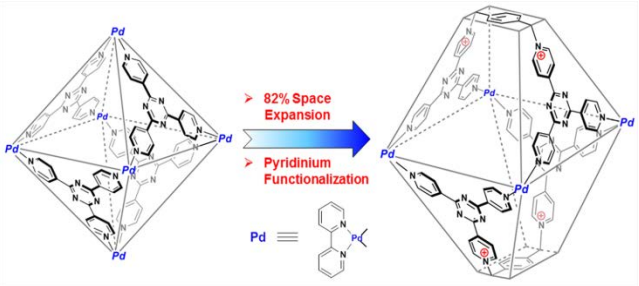


Herein, we report the self-assembly, photochromic, redox and host-guest functions of a $Pd_4L_2$-type nanocapsule (**2**) made of four cis-blocked palladium corners and two pyridinium-functionalized bis-bidentated ligand (**1**), which is synthesized from two 2,4,6-tris(4-pyr-idyl)-1,3,5-triazine (TPT) with a *p*-xylene linker (Scheme 1). As a near relative of the previous $Pd_6L_4$ cage (**3**) reported by Fujita group,[2e, 10] the present $Pd_4L_2$ cage keeps highly +12 charged thus is expected to be highly water-soluble. Moreover, introduction of pyridinium moieties not only enhances the electron-deficient nature of the TPT panels, but also imparts photochromic and redox activities into the cage. Meanwhile, the cavity of **2** is also expanded by insertion of two *p*-xylene spacers. All the above characteristics are subsequently used to the guest-encapsulation studies of **2** toward a series of neutral aromatic compounds and anionic POM clusters. It is noticed that in case of POMs@**2**, the host-guest complexes can still have extra space for

aromatic thiolester substrates, while no ternary complexes are observed in case of POMs@**3**. Desulfurization catalytic properties of the POMs@**2** are then demonstrated, featuring much improved conversion and product (sulfoxide/sulfone) selectivity.

## RESULTS AND DISCUSSION

**Self-assembly and X-ray crystal structure of cage 2**. Ligand **1** ($BF_4^-$ salt**)** was obtained in 87.5% yield by heating 3.5 equiv of TPT with 1,4-bis(bromo-methyl)benzene at 120 °C for 24 h in dimethylformamide followed by counter-ion exchange with excess of $NaBF_4$ (Figure 1A). Molecular formula of ligand **1** has been confirmed by NMR, ESI-TOF mass spectroscopy (Figures S1-4).Cage **2** was successfully self-assembled when a suspension of ligand **1** (12 μmol) was treated with $(bpy)Pd(NO_3)_2$ (24 μmol) in $D_2O$ with vigorous stirring at 70 °C for 12 h. $^1H$ NMR spectra confirmed the quantitative formation of **2** and all the proton signals were fully assigned based on a $^1H$–$^1H$ COSY experiment (Figures S5, and S8). The downfield-shifting of the pyridyl doublets (9.34 and 9.31 ppm for $H_a$, 9.17 and 8.85 ppm for $H_b$) and the pyridinium doublets (9.55 ppm for $H_d$ and 8.97 ppm for $H_c$) compared to that on free ligand **1** indicated the complexation with palladium. Appearance of only one set of signals for the ligands indicates the high symmetry of complex **2** (Figure 1B, 1C). Diffusion-ordered spectroscopy (DOSY) NMR spectrum also confirmed the formation of a single species with diffusion coefficient of $1.32\times10^{-10}$ $m^2s^{-1}$, corresponding to a diameter of 1.9 nm (Figure 1D).

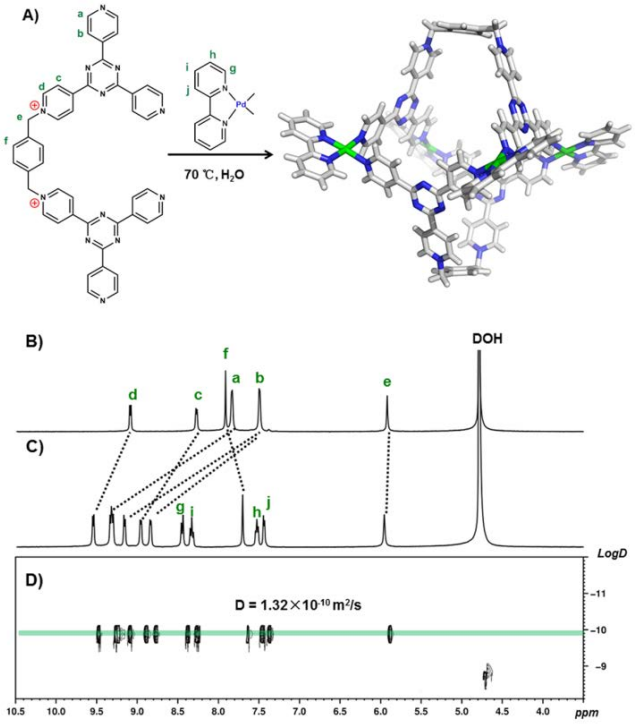


**Figure 1** A) Self-assembly of cage **2** form ligand **1**, where X-ray crystal structure of cage **2** is shown (counter ions and solvent molecules are omitted for clarity), $^1H$ NMR spectra (400 MHz, $D_2O$, 298 K) of B) ligand **1** and C) cage **2,** D) $^1H$ DOSY spectrum of cage **2**.

The structure of cage **2** was then unambiguously determined by synchrotron X-ray crystallographic analysis. Colorless single crystals, suitable for X-ray crystallography, were obtained by vapor diffusion of acetone into an aqueous solution of **2** over one week. In the crystal structure, two cationic pyridinium ligands are connected by four square-planar coordinated Pd(II) ions which are cis-capped by bpy ligands. As depicted in Figure 1A, four Pd(II) ions sitting in the middle the diagonal Pd-Pd distance is 1.93 nm, which is consistent with the known crystal structures of $Pd_6L_4$ cage **3**.[10c,10d,11] However, the cavity of cage **2** is expanded due to the introduction of two *p*-xylene spacers, which could be regarded as two frusta solid packed together in the bottom-to-bottom manner. The center-to-center distance between the two truncated benzenoid planes is ca. 2.04 nm (Figure S10). Based on such estimation, the cavity of cage **2** is ca. 1.8 times larger than the parent cage **3**. Such a great size-expansion, along with the formation of strongly electron-deficient pyridinium rings on the TPT panels, are expected to exert dramatic influence on the host-guest properties of the cage.

**Host-guest studies**. Guest encapsulation properties in water for both cage **2** and cage **3** were firstly compared with a series of aromatic molecules including polycyclic aromatic hydrocarbons (PAHs: naphthalene and pyrene), thiolesters (DBT: dibenzothiophene; DPS: diphenyl sulfide; MBT: thioanisole). Excess amount of guest (10-20 equiv) was added as solid to a $D_2O$ solution of the host (2 mM) and the mixture was stirred for 3 h before subjected to NMR measurement. During stirring, the colorless cage solution changed gradually from to yellow or orange. Due to poor water-solubility of these aromatic molecules (except for DPS and MBT), they could hardly be detected by $^1H$ NMR spectroscopy when suspended in $D_2O$. However, formations of host-guest complexes were evidenced by NMR spectra (Table 1, Figure 2 and Figures S11-21 ). In the presence of the supermolecular cages, clearly upfield-shifted guest signals were visible, from which guest encapsulation was inferred to have taken place inside the hydrophobic cavity.[12] It is worth to note that in most cases, an increased number of guest molecules can be accommodated by cage **2** than cage **3**. For example, based on the NMR integration, three naphthalene molecules can be encapsulated by cage **2**, while cage **3** can hold only up to two such guests (Figure S28). Similarly, one pyrene molecule can be trapped inside cage **2** but by a clear contrast, no binding is observed with cage **3** (Figure S27). In the case of DBT, a 1:3 host-guest complex of $(DBT)_3$@**2** was quantitatively formed while no encapsulation of DBT in cage **3** was inferred to take place as neither significant shifts of host nor guest NMR signals were observed (Figure S27). From these results, we conclude that the newly designed cage **2** inherently bears more space and has a greater potential than cage **3** in guest-uptake.

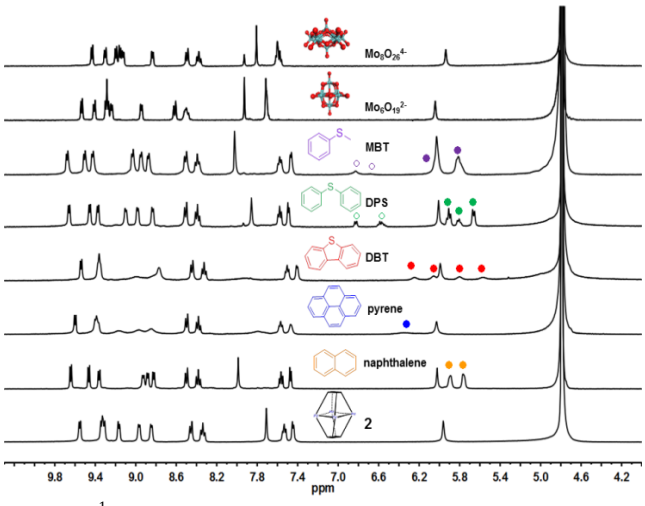


**Figure 2** $^1H$ NMR spectra of cage **2** and the host-guest complexes (400 Hz, $D_2O$, 298 K). Guest signals are represented as circles: the hollow circles represent free guests (or external binding) in solution; solid circles represent guests encapsulated in the cavity.

**Table 1. Summary of guests studied and their encapsulation numbers in both cage 2 and 3.**

| Guests | Encapsulation numbers[a] | |
|---|---|---|
| | Cage **3** | Cage **2** |
| Naphthalene | 2 | 3 |
| Pyrene | 0[b] | 1 |
| Dibenzothiophene | 0 | 3 |
| Diphenyl sulfide | 2 | 2 |
| Thioanisole[c] | - | - |
| $Mo_6O_{19}^{2-}$ | 1 | 2 |
| $Mo_8O_{26}^{4-}$ | 1 | 1 |
| $PMo_{12}O_{40}^{3-}$ | 0 | 0 |

[a]Guest encapsulation numbers within the cavity were obtained from NMR titration and integral ratio.[b]The pyrene molecule cannot be encapsulated alone in the cage **3** unless it is co-encapsulated with another small molecule: see Reference[13]. [c] MBT inclusion is in fast equilibration.

The solid state structure of the inclusion complex $(DBT)_3$@**2** has also been revealed by X-ray crystallographic analysis (Figure 3). Suitable crystals were obtained by slow evaporation of an aqueous solution of the host-guest complex. The structure of $(DBT)_3$@**2** shows that three DBT molecules are sitting inside cage **2** by stabilization of π-π stacking interactions between DBT molecules and the TPT panels of the cage.

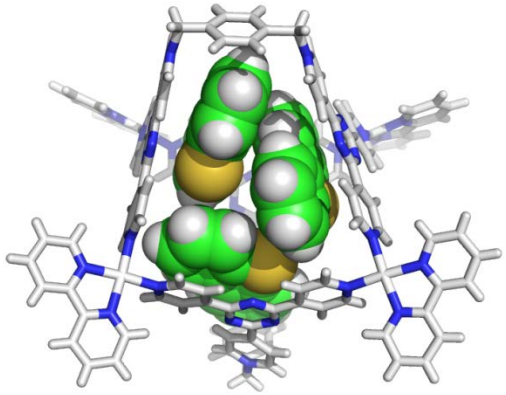

**Figure 3** X-ray structure of $(DBT)_3$@2. For clarity, anions and water molecules have been omitted. Only one set of the disordered DBT (spheres: C, green; H, white; S, yellow) molecules is shown.

Beside organic guests, three POMs anions with increasing size, from $Mo_6O_{19}^{2-}$, $Mo_8O_{26}^{4-}$ to $PMo_{12}O_{40}^{3-}$ (tetrabutylammonium salts) are also chosen as candidates for host-guest studies, due to their wide utilization and excellent chemical activity.[8d,14] $^1$H NMR titrations experiments were performed by adding different ratios of POMs to the solution of cage **2**. The DOSY spectra for the POMs@cage complexes have also been measured (Figures S22-23), where similar diffusion constants are consistent with the other host-guest complexes.The new upfield shifted signals of the cage, especially protons on the cavity surface ($H_c$, $H_d$, $H_e$ and $H_f$) rather than the periphery bpy cis-capping ligands were observed once after the first 0.5 equiv of $Mo_6O_{19}^{2-}$ was added, indicating the successful inclusion of the $Mo_6O_{19}^{2-}$ inside the cavity near the two pyridinium functionalized corners. Strong binding was indicated by the lack of fast equilibrium, where two distinct sets of signals assignable to both empty cage and the inclusion complex are observed. Further increase of $Mo_6O_{19}^{2-}$ anions confirmed that a 1:2 inclusion complex $(Mo_6O_{19}^{2-})_2$@**2** is formed (Figure S32).

As no host-guest complexes are crystallized, we infer that close electro-static and anion-π interactions between the pyridinium panels and $Mo_6O_{19}^{2-}$ are the main driving-forces for the host-guest complex formation. Different from the hydrophobic binding of neutral aromatic compounds which happens only in aqueous solution, uptake of POMs by cage **2** proceeds even in organic solvents, such as $CH_3CN$ (Figure S33).

We also noted that sizes of the window and the inner cavity determined the POM binding properties of cage **2**. When it comes to the $Mo_8O_{26}^{4-}$ cluster, which is slightly larger than $Mo_6O_{19}^{2-}$ (with diameters of 8.3 Å and 8.0 Å, correspondingly, Figure S31), a 1:1 inclusion complex $Mo_8O_{26}^{4-}$@**2** was formed (Figure S34). It is worth to mention that 1:1 host-guest complexes for $Mo_6O_{19}^{2-}$ and $Mo_8O_{26}^{4-}$ with cage **3** were observed (Figures S36 and S37). Meanwhile, strong de-symmetrization of the host NMR signals on these two host-guest complexes suggests that cavity of cage **3** is very limited for the theses cluster anions, where the tumbling motion is restrained on the NMR time-scale. While, the Keggin-type $PMo_{12}O_{40}^{3-}$ with a larger size of 10.5 Å can not be encapsulated in neither cage **2** or cage **3** (Figure S35 and S38). We also noticed that the larger space offered by cage **2** is beneficial for co-encapsulation of both organic and inorganic guest molecules (see discussion below).

**IR, UV-Vis spectra, diffuse reflectance, and ESR studies.** The solids of host-guest complexes were obtained by evaporation of aqueous solution of host-guest complexes. In the IR spectra of ligand **1** and cage **2**, the C=N bond stretching vibration υ (C=N) of the pyridinium ring appeared at ~1644 $cm^{-1}$. As for the $(Mo_6O_{19}^{2-})_2$@**2** and $Mo_8O_{26}^{4-}$@**2** host-guest complexes, the characteristic peaks of υ (Mo=O) and υ (O-Mo-O) in the region 960-550 $cm^{-1}$ confirmed the formation of binary inclusion complexes **(**Figure S39**)**. The UV-Vis absorption spectra for the solution of inclusion complexes with neutral aromatic molecules showed a new charge transfer (CT) absorption band in the range of 315-400 nm, derived from π-stacking interaction between host and aromatic guest (Figures S40-41). Similarly, UV-Vis spectra also support the formation of host-guest complexes with the POM clusters, $(Mo_6O_{19}^{2-})_2$@**2** and $Mo_8O_{26}^{4-}$@**2**, in aqueous solution (Figure S42), where a new CT band at around 321 nm observed due to the interaction between the electron-rich POMs and the electron-deficient pyridinium-based ligands of cage.[15]

Photochromic behaviors of cage **2** and POMs@**2** in the solid state have been investigated. Only weak color change for cage 2 has been observed after irradiation (Figure S45). Interestingly, the light-yellow solids of both POMs@**2** inclusion complexes turned pale blue upon irradiation with a xenon lamp in air at room temperature. The diffuse reflectance spectra display new absorption bands at 407 nm, 718 nm and 1057 nm for $(Mo_6O_{19}^{2-})_2$@**2**, and 406 nm, 715 nm and 1053 nm for $Mo_8O_{26}^{4-}$@**2** after irradiation (Figures 4A and S43). The appearance of a shoulder peak around 407 nm also support the existence of stronger intermolecular CT interactions. The other two long wavelength bands are attributed to the generation of pyridinium radicals after photo-irradiation, giving rise to the color change of $(Mo_6O_{19}^{2-})_2$@**2** and $Mo_8O_{26}^{4-}$@**2** (Figures 4A inset).

Indeed, generation of the radicals was then confirmed by electron spin resonance spectroscopy (ESR). ESR spectra (solid, 298K) of cage 2 have also been checked, again with slight change observed after the irradiation. In sharp contrast，ESR studies before and after irradiation show that light-yellow solid samples of $(Mo_6O_{19}^{2-})_2$@**2** and $Mo_8O_{26}^{4-}$@**2** are almost ESR-silent while the pale blue ones are ESR-active, giving resonance signals at g =2.0038 and 2.0039, respectively (Figure 4B). Another broad

signals at g = 1.9288 and 1.9263 were also observed, which consists well to the value for ESR signal of $Mo_6O_{19}^{3-}$ (with a $Mo^V$ nuclei spin I = 5/2 center, Figure S44).[16] Photochromic properties in anaerobic aqueous solution were also investigated. The same radical species was generated in the solution of $(Mo_6O_{19}^{2-})_2$@**2** since the solution also quickly turned blue upon irradiation under nitrogen atmosphere. The radical species was rather stable as the colour remain unchanged for more than 3 days at room temperature. ESR analysis of the blue species in frozen aqueous solution (100 K) showed splitting signals at g = 2.0110 and g = 1.9273 (Figure S46), which was an obvious evidence that $Mo^V$ magnetically interacts with the radical species generated by cage **2**.[17] We infer that the interaction between the electron-rich POMs donor and pyridinium acceptor moieties is responsible for the enhanced photochromic behavior of POMs@cage complexes. We also found the generation of radical species in the solution of the host-guest complex $(DBT)_3$@2 (Figure S47), indicative of the main role of host-guest interaction on the formation of pyridinium radicals.

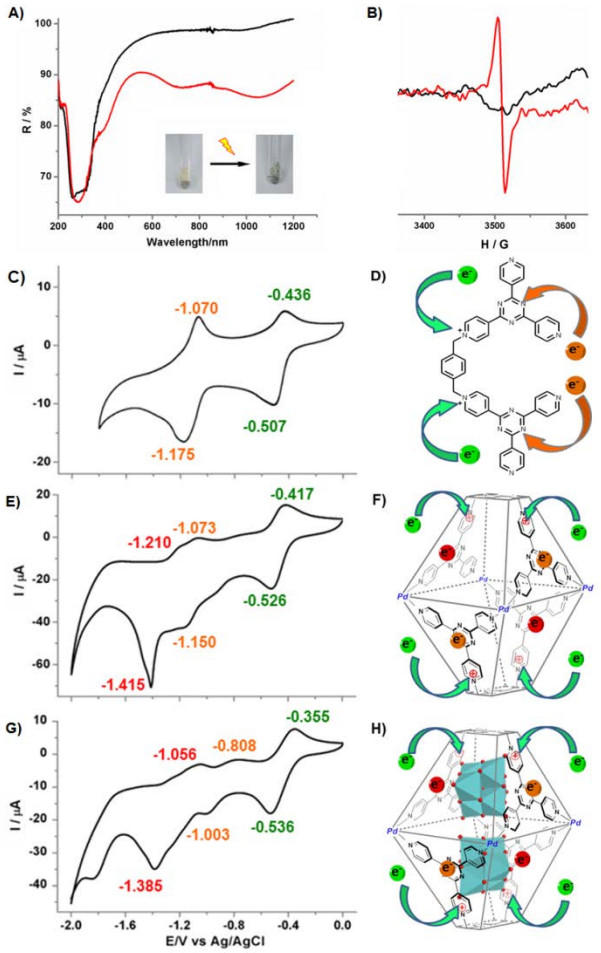


**Figure 4** A) UV–vis diffuse reflectance spectra (with insets showing the photos of the sample before and after the photo-irradiation) and B) ESR spectra for $(Mo_6O_{19}^{2-})_2$@**2** before (black line) and after (red line) photo-irradiation (xenon lamp; 200 mW/cm$^2$). Cyclic voltammograms of C) ligand **1** (1 mM), E) cage **2** (0.5 mM), G) $(Mo_6O_{19}^{2-})_2$@**2** (0.05 mM, MeCN) with D, F, H) showing the corresponding oxidation states for each reduction waves. The CVs were recorded in a 0.1 M solution of $Bu_4NPF_6$ electrolyte at a scan rate of 100 mV/s.

**Cyclic voltammetry**. Cyclic voltammetry (CV) experiments have been carried out to elucidate the redox properties of cage **2** and the host-guest complexes (Figure 4C-H). The CVs of ligand **1** and cage **2** in MeCN containing 0.1 M tetra(n-butyl)ammonium hexafluorophosphate ($TBAPF_6$ electrolyte) are compared in Figures 4C and 4E with a scan rate of 100 mV/s. Two reversible reduction waves for ligand **1** were observed at around -0.507 V and -1.175 V vs. Ag/AgCl. The first reduction potential for ligand **1** (-0.507 V) is attributed to the two-electron reduction process on both pyridinium units to form neutral state $\mathbf{1}^0$, which is typical for pyridinium derivative.[18] The second more negative one (-1.175 V) is assigned to the formation of $\mathbf{1}^{2-}$ dianion due to the electron accepting triazine unit (Figure 4D).[19] In the CV of cage **2**, the first reduction potential appeared at more negative positions (-0.526 V) than that of ligand **1**, indicating cage **2** formed by two dicationic ligands maintains the redox characteristics of pyridinium derivatives, but being more difficult to be reduced after coordination to Pd(II). The second (-1.150 V) and third reduction waves (-1.415 V) are assigned to the two two-electron reduction processes on the triazine units, particularly the latter is negatively shifted as compared with that of the ligand $\mathbf{1}^0/\mathbf{1}^{2-}$ reduction. This observation is consistent with a previous report: the triazine unit in the cage skeleton can extend the redox behavior down into the anionic regime, which also indicates inter-ligand electronic communications between the triazine panels are taking place through the coordination bonds.[5b] It has to be pointed out that without the pyridinium functional moieties, cage **3** has been proved to be unstable below -0.8 V as CV showed irreversible redox waves under similar conditions.[20]

As for the $(Mo_6O_{19}^{2-})_2$@**2** host-guest complex, the half wave potential $[E_{1/2}=(E_{pa}+E_{pc})/2]$ for the first redox waves is found to be -0.445V, which is a bit larger than the value of empty cage 2 (-0.471V). The other two redox waves were shifted to more positive potentials (Figure 4G) compared to those observed for the empty cage **2**, indicating that encapsulation of POM inside **2** makes the thiazine units on the ligands much easier to be reduced. It is worth mentioning that both inclusion complexes $(Mo_6O_{19}^{2-})_2$@**2** and $Mo_8O_{26}^{4-}$@**2** present quasi-reversible or a totally irreversible wave (Figure S48), which indicates the presence of the electron-rich POM anions significantly alters the stability of the radical ion species formed in the reduction process.

We also investigated the CVs of cage **2** and binary complexes $(DBT)_3$@**2** and pyrene@**2** in $H_2O$ solution containing 30 mM $NaNO_3$ as electrolyte (Figures S49-51). The concentration of complexes in aqueous solution and scan rate were the same as that in MeCN solution. Cage **2** showed only one broad reversible reduction peak at -0.452 V, higher than that observed in MeCN solution. It seems that simultaneous reduction process occurred in aqueous solution. The half wave potential $E_{1/2}$ (-0.340 V) is less anodic, indicating that the solvent medium has an important effect on electrochemical behavior of cage **2**. The CV of $(DBT)_3$@**2** shows three irreversible reduction waves at around -0.491 V, -0.680 V, and -0.861 V. Similar irreversible processes took place in the CV of pyrene@**2,** except that the third reduction wave was observed at -0.933 V, more negatively shifted compared with that of $(DBT)_3$@**2.** We infer that the radical species formed in the reduction process are not stable and have been consumed once reduced. Further studies are currently underway to address the electrochemical reaction details for these complexes.

**Catalytic properties of POMs@2 host-guest complexes.** It is well known that POMs are preponderant catalysts on oxidation reactions of alkenes, alkanes, nitrogen- and sulfur-containing compounds et al.[8b,21] Oxidative desulfurization reactions, which are considered to be promising strategy to remove refractory sulfur containing compounds in fuels[22] have been chosen as proof-of-concept model reactions to investigate the catalytic property of our inclusion complexes of POMs@**2**.

Diphenylsulfide (DPS) was selected as the representative substrate for discussion below. When suspending DPS (1.90 mg, 0.01 mmol) in an $D_2O/CD_3CN$ (V/V=5:1) solution of the binary complex $Mo_8O_{26}^{2-}$@**2** (2 mM, 0.5 mL) at room temperature, $^1H$ NMR spectrum showed that the signals strikingly changed and guest signals assignable to the DPS substrates were observed with smaller downfield-shifting compared to the guest chemical shifts in the $(DPS)_2$@**2** complex, which indicates that fast exchanging ternary guest binding process occurred within the expanded hydrophobic space of cage **2**. In contrast, no co-encapsulation was observed when $Mo_8O_{26}^{2-}$@**3** was tested, where instead replacement of the $Mo_8O_{26}^{2-}$ guest by DPS happened **(**Figures S52-57).

After removing the excess guest molecules by filtration, the resulting (DPS+$Mo_8O_{26}^{2-}$)@**2** solution was heated at 60°C for 9 h with the addition of an excess amount of t-butyl hydroperoxide (TBHP, ca. 31 equiv) as the oxidant. After reaction, NMR signals of DPS molecules disappeared, meanwhile new signals assignable to the diphenylsulfoxide (DPSO) product appeared (Figure 5C). Based on NMR and GC-MS analysis (Figure 5D, Figure S72), the

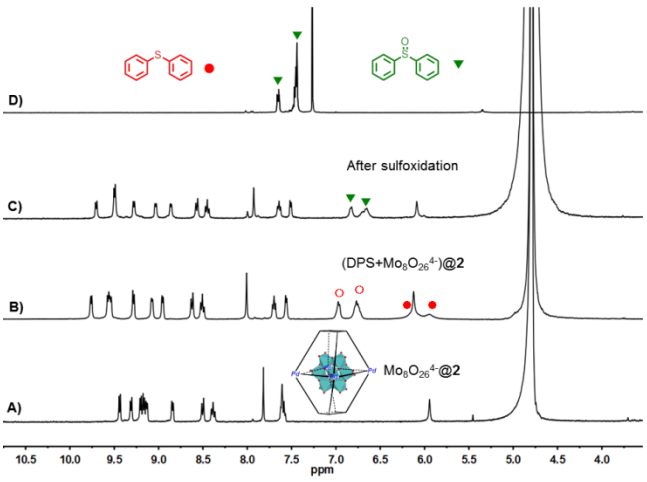


**Figure 5** $^1H$ NMR spectra (400 MHz, 298 K) of a 1 mM solution of A) $Mo_8O_{26}^{4-}$@**2** in $D_2O/CD_3CN$(5/1), (B) ternary complex obtained by adding DPS to the solution of $Mo_8O_{26}^{4-}$@**2** and C) after sulfoxidation reaction in $D_2O/CD_3CN$ (V/V=5/1), D) crude product extracted to $CDCl_3$. The signals of DPS and DPSO are represented by (●) and (▼), respectively. The doublet signals at 6.83 ppm and multiple signals at around 6.58 ppm are free DPS dissolved in $D_2O$, denoted by(○).

substrate was fully consumed and converted mostly into DPSO (100% conversion, 95.0% chemoseletivity, table 2, entry 1). When $(Mo_6O_{19})_2$@**2** was used as the catalyst, the DPS to DPSO reaction witnessed high conversion (100%) but slightly lower (75 %) chemoseletivity (entry 2, Figures S62 and S73).[21b]

To investigate the turnover number of POMs@**2** catalyst, 10 mol% of $Mo_8O_{26}^{2-}$@**2** was then tested to catalyze the sulfoxidation of DPS. After 17 hours of stirring under the same condition, we obtained conversion of 96.2% corresponding to a turn-over number of 9.6, giving again the sulfoxide as the main product (88.9% selectivity, entry 3 in Table 2). In order to complete the catalytic cycle, the inclusion of substrate and exclusion of product must be fulfilled to ensure the turnover of catalysis.[23] Competitive guests binding between DPS and DPSO with POMs@**2** were studied by NMR titration, which showed that POMs@**2** has weaker binding ability toward DPSO (Figures S58-59). This difference in binding strength comes from the hydrophilic S=O moiety of product, resulting in the reduced host-guest hydrophobic interaction to facilitate the replacement of the DPSO product by DPS in the cage cavity. The disappearance of DPS signals and increasement and downfield-shift of DPSO signals with the reaction time also provided strong evidence to explain turnover and selectivity (Figture S61).

As control experiments (see entry 4 and 5 in Table 2), we also examined the oxidation of DPS with $(n\text{-}Bu_4N)_4[Mo_8O_{26}]$ and $(n\text{-}Bu_4N)_2[Mo_6O_{19}]$ as catalysts in water, which gave much lower conversions (37.6% and 37.0%, respectively) and product selectivity (81.8% and 80.0%, respectively). Direct oxidation of DPS catalyzed by cage **2** only was also performed, which resulted in only 10% conversion (entry 6). Sulfoxidation of DPS with none catalyst was also performed in $H_2O$ which only gave trace product (5% conversion, entry 7). Similarly, other sulfoxidation experiments of DBT and MBT suggest that POMs@**2** showed high conversion and selectivity to form corresponding sulfoxides (entry 8-13 in Table 2, Figures S64-71).

Based on the results above, a plausible mechanism was proposed for the selective desulfurization catalysis: i) the big hydrophobic cavity of cage **2** leads to an increased solubility of the

**Table 2**. Sulfoxidation of sulfides to sulfoxide and sulfones catalyzed by POMs@cage **2** complexes with TBHP[a].

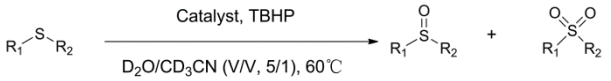


| Entry | Sulfide | Time | Catalyst (loading equiv.) | Conversion % (Selectivity %)[b] |
|---|---|---|---|---|
| 1 | DPS | 9h | $Mo_8O_{26}^{4-}$@**2** (1)[d] | 100 (95.0) |
| 2 | DPS | 9h | $(Mo_6O_{19}^{2-})_2$@**2** (0.5)[d] | 100 (75.0) |
| 3 | DPS | 10h | $Mo_8O_{26}^{4-}$@**2** (0.1)[c] | 96.2 (88.9) |
| 4 | DPS | 10h | $Mo_8O_{26}^{4-}$ (0.1)[c] | 37.6 (81.8) |
| 5 | DPS | 10h | $Mo_6O_{19}^{2-}$ (0.1)[c] | 37.0 (80.0) |
| 6 | DPS | 10h | Cage **2** (0.1)[c] | 10.0 (100) |
| 7 | DPS | 10h | None | 5.0 (71) |
| 8 | DBT | 9h | $Mo_8O_{26}^{4-}$@**2** (0.5)[d] | 93.8 (85.7) |
| 9 | DBT | 9h | $(Mo_6O_{19}^{2-})_2$@**2** (0.5)[d] | 89.6 (93.7) |
| 10 | DBT | 16h | $Mo_8O_{26}^{4-}$@**2** (0.1)[c] | 51.0 (81.0) |
| 11 | MBT | 9h | $Mo_8O_{26}^{4-}$@**2** (0.2)[d] | 100 (83.6) |
| 12 | MBT | 9h | $(Mo_6O_{19}^{2-})_2$@**2** (0.1)[d] | 100 (92.0) |
| 13 | MBT | 16h | $Mo_8O_{26}^{4-}$@**2** (0.1)[c] | 100 (90) |

[a]Reaction conditions: sulfide (0.01 mmol, 10 equiv) was added to catalysts (1 equiv) in $D_2O/CD_3CN$ (V/V=5:1) and then stirred at r.t. for 5 hours, after which insoluble substrates were removed by filtration. Then TBHP (4 mg, 70% in $H_2O$) was added and the solution was heated to 60 °C overnight. [b]The conversion of sulfoxidation reactions are determined using 1,3,5- trimethoxybenzene as the internal standard (Figures S72-84). Selectivity is calculated as SO/(SO + $SO_2$) and determined by $^1H$ NMR and GC-MS. [c]Reaction in water without removal of the excess guest molecules, with 10 mol% catalyst loading. [d]The catalysis loading depend on the encapsulation number of sulfides, see Figures S60-71.

substrate in water; ii) co-encapsulation of POMs and the organic substrates inside cage **2** enhances the effective local concentration and forced the bimolecular collision; iii) selectivity enhancement is realized by the favorable binding of substrates over the sulfoxide products.

## CONCLUSIONS

In conclusion, a water-soluble redox-active $Pd_4L_2$ cage featuring enlarged pore-opening and internal cavity is obtained. The expanded hydrophobic cavity of this new generation of organopalladium cage can preferentially encapsulate hexamolybdate and octamolybdate cluster anions, leaving additional room for the co-encapsulation of sulfides substrates. CV study showed the redox-activity of the cage and the binary inclusion complexes derived from the pyridinium moieties on the ligand. Sulfoxidation reactions catalyzed by binary POMs@cage complexes exhibited enhanced conversion and chemoselectivity compared to the POMs

or cage only. The current study provides a general and valuable strategy for expanding the stability, product selectivity of classical transition-metal catalysts in water.

## ASSOCIATED CONTENT

Full synthetic and structural details, crystallographic data (CIF), and supplemental figures and tables as described in the text. This material is available free of charge via the Internet at http://pubs.acs.org.

## AUTHOR INFORMATION

### Corresponding Author

*qfsun@fjirsm.ac.cn

### Notes

All authors have given approval to the final version of the manuscript.

## ACKNOWLEDGMENT

Dedicated to prof. Xin-Tao Wu on the occasion of his 80th birthday. This work was supported by the National Natural Science Foundation of China (Grant nos. 21521061, 21471150, 21601183), the Strategic Priority Research Pro-gram of the Chinese Academy of Sciences (Grant No. XDB20000000), Natural Science Foundation of Fujian Province (Grant nos. 2016J06005, 2016J05051, 2017J05037). We thank the staff of BL17B beamline at the National Centre for Protein Sciences Shanghai and Shanghai Synchrotron Radiation Facility, Shanghai, PR China, for assistance during data collection.

## REFERENCES

(1) (a) Harris, K.; Fujita, D.; Fujita, M. *Chem. Commun.* **2013**, *49*, 6703. (b) Cook, T. R.; Stang, P. J. *Chem. Rev.* **2015**, *115*, 7001. (c) Castilla, A. M.; Ramsay, W. J.; Nitschke, J. R. *Acc. Chem. Res.* **2014**, *47*, 2063. (d) Chakrabarty, R.; Mukherjee, P. S.; Stang, P. J. *Chem. Rev.* **2011**, *111*, 6810. (e) Han, M.; Engelhard, D. M.; Clever, G. H. *Chem. Soc. Rev.* **2014**, *43*, 1848. (f) Sun, Q. F.; Sato, S.; Fujita, M. *Angew. Chem. Int. Ed.* **2014**, *53*, 13510. (g) Northrop, B. H.; Zheng, Y.-R.; Chi, K.-W.; Stang, P. J. *Acc. Chem. Res.* **2009**, *42*, 1554. (h) Cook, T. R.; Vajpayee, V.; Lee, M. H.; Stang, P. J.; Chi, K.-W. *Acc. Chem. Res.* **2013**, *46*, 2464. (i) Liu, J.; Chen, L.; Cui, H.; Zhang, J.; Zhang, L.; Su, C.-Y. *Chem. Soc. Rev.* **2014**, *43*, 6011. (j) Oliveri, C. G.; Ulmann, P. A.; Wiester, M. J.; Mirkin, C. A. *Acc. Chem. Res.* **2008**, *41*, 1618. (k) Saha, M. L.; De, S.; Pramanik, S.; Schmittel, M. *Chem. Soc. Rev.* **2013**, *42*, 6860. (l) Smulders, M. M. J.; Riddell, I. A.; Browne, C.; Nitschke, J. R. *Chem. Soc. Rev.* **2013**, *42*, 1728. (m) Bloch, W. M.; Clever, G. H. *Chem. Commun.* **2017**, *53*, 8506. (n) Han, Y.-F.; Jia, W.-G.; Yu, W.-B.; Jin, G.-X. *Chem. Soc. Rev.* **2009**, *38*, 3419.

(2) (a) Sawada, T.; Yoshizawa, M.; Sato, S.; Fujita, M. *Nat. Chem.* **2009**, *1*, 53. (b) Klosterman, J. K.; Yamauchi, Y.; Fujita, M. *Chem. Soc. Rev.* **2009**, *38*, 1714. (c) Li, K.; Zhang, L. Y.; Yan, C.; Wei, S. C.; Pan, M.; Zhang, L.; Su, C. Y. *J. Am. Chem. Soc.* **2014**, *136*, 4456. (d) Zhang, Y.-Y.; Gao, W.-X.; Lin, L.; Jin, G.-X. *Coordin. Chem. Rev.* **2017**, *344*, 323. (e) Yoshizawa, M.; Klosterman, J. K.; Fujita, M. *Angew. Chem. Int. Ed.* **2009**, *48*, 3418. (f) Dong, S.; Luo, Y.; Yan, X.; Zheng, B.; Ding, X.; Yu, Y.; Ma, Z.; Zhao, Q.; Huang, F. *Angew. Chem. Int. Ed.* **2011**, *50*, 1905. (g) Zhang, W.-Y.; Lin, Y.-J.; Han, Y.-F.; Jin, G.-X. *J. Am. Chem. Soc.* **2016**, *138*, 10700. (h) Jiang, B.; Wang, W.; Zhang, Y.; Lu, Y.; Zhang, C.-W.; Yin, G.-Q.; Zhao, X.-L.; Xu, L.; Tan, H.; Li, X.; Jin, G.-X.; Yang, H.-B. *Angew. Chem. Int. Ed.* **2017**, *56*, 14438.

(3) (a) Brown, C. J.; Toste, F. D.; Bergman, R. G.; Raymond, K. N. *Chem. Rev.* **2015**, *115*, 3012. (b) D. Fiedler, D. H. L.; R. G. Bergman, a.; Raymond, K. N. *Acc. Chem. Res.* **2005**, *38*, 351. (c) Preston, D.; Lewis, J. E. M.; Crowley, J. D. *J. Am. Chem. Soc.* **2017**, *139*, 2379. (d) Chen, S.; Li, K.; Zhao, F.; Zhang, L.; Pan, M.; Fan, Y. Z.; Guo, J.; Shi, J.; Su, C. Y. *Nat. Commun.* **2016**, *7*, 13169. (e) Bloch, W. M.; Abe, Y.; Holstein, J. J.; Wandtke, C. M.; Dittrich, B.; Clever, G. H. *J. Am. Chem. Soc.* **2016**, *138*, 13750. (f) Stang, P. J.; Olenyuk, B. *Acc. Chem. Res.* **1997**, *30*, 502. (g) McConnell, A. J.; Wood, C. S.; Neelakandan, P. P.; Nitschke, J. R. *Chem. Rev.* **2015**, *115*, 7729. (h) Pluth, M. D.; Bergman, R. G.; Raymond, K. N. *Acc. Chem. Res.* **2009**, *42*, 1650. (i) Guo, J.; Xu, Y.-W.; Li, K.; Xiao, L.-M.; Chen, S.; Wu, K.; Chen, X.-D.; Fan, Y.-Z.; Liu, J.-M.; Su, C.-Y. *Angew. Chem. Int. Ed.* **2017**, *56*, 3852. (j) Tan, C.; Jiao, J.; Li, Z.; Liu, Y.; Han, X.; Cui, Y. *Angew. Chem. Int. Ed.* **2018**, *57*, 2085. (k) Jiao, J.; Tan, C.; Li, Z.; Liu, Y.; Han, X.; Cui, Y. *J. Am. Chem. Soc.* **2018**, *140*, 2251. (l) Luo, D.; Wang, X.-Z.; Yang, C.; Zhou, X.-P.; Li, D. *J. Am. Chem. Soc.* **2018**, *140*, 118. (m) Chen, H.; Huang, Z.; Wu, H.; Xu, J.-F.; Zhang, X. *Angew. Chem. Int. Ed.* **2017**, *56*, 16575.

(4) (a) Kurihara, K.; Yazaki, K.; Akita, M.; Yoshizawa, M. *Angew. Chem. Int. Ed.* **2017**, *56*, 11360. (b) Yazaki, K.; Kishi, N.; Akita, M.; Yoshizawa, M. *Chem. Commun.* **2013**, *49*, 1630. (c) Wang, Y.; Sun, J.; Liu, Z.; Nassar, M. S.; Botros, Y. Y.; Stoddart, J. F. *Angew. Chem. Int. Ed.* **2016**, *55*, 12387. (d) Roy, B.; Zangrando, E.; Mukherjee, P. S. *Chem. Commun.* **2016**, *52*, 4489. (e) Mukherjee, S.; Mukherjee, P. S. *Chem. Commun.* **2014**, *50*, 2239. (f) Xu, L.; Wang, Y.-X.; Chen, L.-J.; Yang, H.-B. *Chem. Soc. Rev.* **2015**, *44*, 2148.

(5) (a) Dale, E. J.; Vermeulen, N. A.; Thomas, A. A.; Barnes, J. C.; Juricek, M.; Blackburn, A. K.; Strutt, N. L.; Sarjeant, A. A.; Stern, C. L.; Denmark, S. E.; Stoddart, J. F. *J. Am. Chem. Soc.* **2014**, *136*, 10669. (b) Hafezi, N.; Holcroft, J. M.; Hartlieb, K. J.; Dale, E. J.; Vermeulen, N. A.; Stern, C. L.; Sarjeant, A. A.; Stoddart, J. F. *Angew. Chem. Int. Ed.* **2015**, *54*, 456.

(6) Bruns, C. J.; Fujita, D.; Hoshino, M.; Sato, S.; Stoddart, J. F.; Fujita, M. *J. Am. Chem. Soc.* **2014**, *136*, 12027.

(7) Yazaki, K.; Noda, S.; Tanaka, Y.; Sei, Y.; Akita, M.; Yoshizawa, M. *Angew. Chem. Int. Ed.* **2016**, *55*, 15031.

(8) (a) Han, Q.; Qi, B.; Ren, W.; He, C.; Niu, J.; Duan, C. *Nat. Commun.* **2015**, *6*, 10007. (b) Wang, S. S.; Yang, G. Y. *Chem. Rev.* **2015**, *115*, 4893. (c) Zheng, S. T.; Yang, G. Y. *Chem. Soc. Rev.* **2012**, *41*, 7623. (d) Dolbecq, A.; Dumas, E.; Mayer, C. R.; Mialane, P. *Chem. Rev.* **2010**, *110*, 6009.

(9) (a) Han, M.; Hey, J.; Kawamura, W.; Stalke, D.; Shionoya, M.; Clever, G. H. *Inorg. Chem.* **2012**, *51*, 9574. (b) Kuang, X.; Wu, X.; Yu, R.; Donahue, J. P.; Huang, J.; Lu, C. Z. *Nat. Chem.* **2010**, *2*, 461. (c) Wu, Y.; Shi, R.; Wu, Y. L.; Holcroft, J. M.; Liu, Z.; Frasconi, M.; Wasielewski, M. R.; Li, H.; Stoddart, J. F. *J. Am. Chem. Soc.* **2015**, *137*, 4111. (d) Guang-Gang, G.; Ping-Shing, C.; Mak, T. C. W. *J. Am. Chem. Soc.* **2009**, *131*, 18257. (e) Gao, G.-G.; Cheng, P.-S.; Mak, T. C. W. *J. Am. Chem. Soc.* **2009**, *131*, 18257. (f) Liu, Y.; Hu, C.; Comotti, A.; Ward, M. D. *Science* **2011**, *333*, 436.

(10) (a) Fujita, M.; Tominaga, M.; Hori, A.; Therrien, B. *Acc. Chem. Res.* **2005**, *38*, 371. (b) M. Fujita; D. Oguro; M. Miyazawa; H. Oka; K. Yamaguchi; Ogura, K. *Nat. Chem.* **1995**, *378*, 469. (c) Nakabayashi, K.; Kawano, M.; Kato, T.; Furukawa, K.; Ohkoshi, S.; Hozumi, T.; Fujita, M. *Chem. Asian. J.* **2007**, *2*, 164. (d) Nakabayashi, K.; Kawano, M.; Yoshizawa, M.; Ohkoshi, S.-i.; Fujita, M. *J. Am. Chem. Soc.* **2004**, *126*, 16694.

(11) Kusukawa, T.; Fujita, M. *J. Am. Chem. Soc.* **2002**, *124*, 13576.

(12) Ronson, T. K.; Meng, W.; Nitschke, J. R. *J. Am. Chem. Soc.* **2017**, *139*, 9698.

(13) Yoshizawa, M.; Tamura, M.; Fujita, M. *J. Am. Chem. Soc.* **2004**, *126*, 6846.

(14) (a) Qin, J. S.; Du, D. Y.; Guan, W.; Bo, X. J.; Li, Y. F.; Guo, L. P.; Su, Z. M.; Wang, Y. Y.; Lan, Y. Q.; Zhou, H. C. *J. Am. Chem. Soc.* **2015**, *137*, 7169. (b) Gao, J.; Cao, S.; Tay, Q.; Liu, Y.; Yu, L.; Ye, K.; Mun, P. C.; Li, Y.; Rakesh, G.; Loo, S. C.; Chen, Z.; Zhao, Y.; Xue, C.; Zhang, Q. *Sci. Rep.* **2013**, *3*, 1853.

(15) Xia, Y.; Wei, Y.; Wang, Y.; Guo, H. *Inorg. Chem.* **2005**, *44*, 9823.

(16) Ian Buckley, R.; Clark, R. J. H. *Coordin. Chem. Rev.* **1985**, *65*, 167.

(17) Ozaki, Y.; Kawano, M.; Fujita, M. *Chem. Commun.* **2009**, 4245.

(18) (a) Jin, X. H.; Chen, C.; Ren, C. X.; Cai, L. X.; Zhang, J. *Chem. Commun.* **2014**, *50*, 15878. (b) Wöß, E.; Monkowius, U.; Knör, G. *Chem. Eur. J.* **2013**, *19*, 1489. (c) Lipke, M. C.; Cheng, T.; Wu, Y.; Arslan, H.; Xiao, H.; Wasielewski, M. R.; Goddard, W. A.; Stoddart, J. F. *J. Am. Chem. Soc.* **2017**, *139*, 3986.

(19) García, A.; Insuasty, B.; Herranz, M. Á.; Martínez-Álvarez, R.; Martín, N. *Org. Lett.* **2009**, *11*, 5398.

(20) Furutani, Y.; Kandori, H.; Kawano, M.; Nakabayashi, K.; Yoshizawa, M.; Fujita, M. *J. Am. Chem. Soc.* **2009**, *131*, 4764.

(21) Zou, C.; Zhang, Z.; Xu, X.; Gong, Q.; Li, J.; Wu, C. D. *J. Am. Chem. Soc.* **2012**, *134*, 87.

(22) (a) Zhu, W.; Li, H.; Jiang, X.; Yan, Y.; Lu, J.; He, L.; Xia, J. *Green Chem.* **2008**, *10*, 641. (b) Yang, C.; Jin, Q.; Zhang, H.; Liao, J.; Zhu, J.; Yu, B.; Deng, J. *Green Chem.* **2009**, *11*, 1401.

(23) (a) Yoshizawa, M.; Tamura, M.; Fujita, M. *Science* **2006**, *312*, 251. (b) Cullen, W.; Misuraca, M. C.; Hunter, C. A.; Williams, N. H.; Ward, M. D. *Nat. Chem.* **2016**, *8*, 231.

SYNOPSIS TOC